

# AUS Repository

## Study of the Electromechanical Models for Cardiac Activity

Item Type	Thesis
Authors	Itani, Rana
Download date	2026-03-16 06:16:28
Link to Item	<a href="http://hdl.handle.net/11073/8850">http://hdl.handle.net/11073/8850</a>

STUDY OF THE ELECTROMECHANICAL MODELS FOR CARDIAC  
ACTIVITY

by  
Rana Itani

A Thesis Presented to the Faculty of the  
American University of Sharjah  
College of Arts and Sciences  
in Partial Fulfillment  
of the Requirements  
for the Degree of  
  
Master of Science in  
Mathematics

Sharjah, United Arab Emirates

May 2017

# Approval Signatures

We, the undersigned, approve the Master's Thesis of Rana Itani.

Thesis Title: Study of the Electromechanical Models for Cardiac Activity.

**Signature**

**Date of Signature**

(dd/mm/yyyy)

---

Dr. Youssef Belhamadia  
Assistant Professor  
Thesis Advisor

---

Dr. Suheil Khoury  
Professor  
Thesis Committee Member

---

Dr. Amjad Tuffaha  
Associate Professor  
Thesis Committee Member

---

Dr. Hana Sulieman  
Head of the Department of Mathematics

---

Dr. James Griffin  
CAS Graduate Programs Director

---

Dr. Mahmoud Anabtawi  
Dean of CAS

---

Dr. Khaled Assaleh  
Interim Vice Provost for Research and Graduate Studies

## **Acknowledgements**

I would like to express my gratitude to my supervisor, Dr. Youssef Belhamadia, whose expertise, suggestions, and patience added considerably to my experience. I have learned a lot from him and without his help I could not have finished my thesis successfully.

I extend my gratitude to my professors in the Department of Mathematics at the American University of Sharjah for their diverse courses, valuable guidance, and cooperation during this amazing journey.

I would like to thank Zainab Rammal, who as a good friend, was believing in me and encouraging me to follow my dreams. She was always there cheering me up, making my time here at AUS a lot more fun.

Finally, I would like to thank my family who were always there standing by me through the good times and bad. For my parents who raised me with a love of science and supported me in all my pursuits.

## Abstract

The mathematical modeling of the complex physical phenomena occurring in the heart is an area of increasing interest, as it facilitates the better understanding of relevant mechanisms driving the behavior of the system in both physiological and pathological contexts. In this work, we are interested in the study of the interaction between the propagation of the electrical potential through the cardiac tissue and the related mechanical response. Two mathematical models for this electromechanical coupling will be presented: the first model is based on an active-stress approach that adds an active contribution to the stress of the material, and the second model is based on an active-strain approach that adopts a multiplicative decomposition of the tensor gradient of deformation. Comparison between these two models and numerical results will be presented illustrating some important features of the cardiac electromechanical coupling.

# Contents

<b>Abstract</b>	<b>4</b>
<b>List of Figures</b>	<b>6</b>
<b>1 Introduction</b>	<b>7</b>
<b>2 Elasticity Theory</b>	<b>10</b>
2.1 Kinematic Relations . . . . .	10
2.2 Stress Equilibrium . . . . .	15
<b>3 Cardiac Mechanics</b>	<b>18</b>
3.1 Active-Strain Approach . . . . .	18
3.2 Active-Stress Approach . . . . .	20
<b>4 Cardiac Electromechanics</b>	<b>23</b>
4.1 Cardiac Electrophysiology . . . . .	23
4.2 Cardiac Electromechanical Coupling . . . . .	24
4.2.1 Active-strain approach . . . . .	24
4.2.2 Active-stress approach . . . . .	25
<b>5 Numerical Simulations</b>	<b>26</b>
5.1 One Dimensional Active-Strain Approach . . . . .	26
5.2 One Dimensional Active-Stress Approach . . . . .	36
5.3 Comparison . . . . .	42
<b>6 Conclusions and Future Work</b>	<b>43</b>
<b>Bibliography</b>	<b>44</b>
<b>Vita</b>	<b>48</b>

## List of Figures

1.1	Simplified diagram of the heart . . . . .	7
2.1	Motion from the reference configuration $\Omega_o$ to the current configuration $\Omega_t$ . . . . .	11
5.1	Deformation corresponding to active-strain approach: Numerical method 1 . . . . .	31
5.2	Deformation corresponding to active-strain approach: Numerical method 2 . . . . .	33
5.3	Deformation corresponding to different values of $\beta$ . . . . .	35
5.4	Deformation corresponding to active-stress approach . . . . .	39
5.5	Deformation corresponding to different values of $K_{T_a}$ . . . . .	41

## Chapter 1: Introduction

The human heart is a pumping organ. This organ is divided into four chambers: upper left atria, lower left atria, upper right ventricle, and lower right ventricle. Where the left part of the heart is responsible of pumping oxygenated blood around the body, however, the right part is responsible of pumping deoxygenated blood to the lungs, (see Figure 1.1). This pumping action is regulated by an electrical signal that propagates through the cardiac tissue causing contraction, and this resulting mechanical activity has also an effect on the electrical propagating signal.

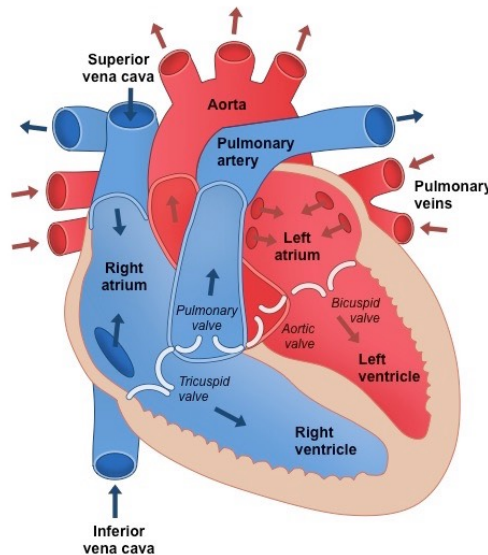


Figure 1.1: Simplified diagram of the heart

<http://ib.bioninja.com.au/standard-level/topic-6-human-physiology/62-the-blood-system/heart-structure.html>

Mathematical modeling of this cardiac electromechanical activity gained a considerable attention in recent years. A lot of effort was dedicated to developing and solving the equations that describe only the electrical activity in the heart (S. Linge et al. [14], R. Clayton et al. [17], P. Pathmanathan et al. [18], R. Clayton and A. Panfilov [20], and the references therein); however, a limited selection of publications is available for understanding the heart mechanics and the coupling of electromechanical activity (M. Nash [7], C. Cherubini [13], D. Ambrosi et al. [21], and the references therein), and that is why the modeling of electromechanical

coupling of the cardiac is still challenging.

In the literature, the first example of a coupled electromechanical model as detailed in a review (N. Trayanova and J. Rice [23]) was proposed by R. Kaufmann et al. [2] (1974), in a mammalian cardiac cells, based on calcium movements, where the behaviour of the model is compared to that of a living cardiac muscle.

Other early electromechanical models include the one by P. Hunter et al. [6] (1998). As mentioned by M. Nash and A. Panfilov [9], this model developed the foundation for electromechanical modelling of the cardiac tissues, where the stress tensor is additively decomposed into its passive and active components, and that is why we will recall it as active-stress based approach. This approach was followed by many researchers. Some of them addressed the stability issue in electromechanical coupled cardiac models (P. Pathmanathan and J. Whitely [16], S. Land et al. [27], and a PhD by N. Kirc [26]), but computational challenges were their major obstacle in modeling despite the advances they made in stabilizing the solution process. Others like A. Panfilov and M. Nash [9] (2004), presented a computational framework to couple a three variables model using the active stress mechanics proposed by P. Hunter et al. [6]. In 2005, A. Panfilov et al. [10] studied the effect of contraction on the dynamics of spiral waves and pacemakers, and in 2007, R. Keldermann et al. [11] found that deformation resulting from this contraction not only include pacemakers but has an effect on spacial organization.

A novel idea can be traced back to the work by P. Nardinocchi and L. Teresi [12] (2007) and C. Cherubini et al. [13] (2008), where the deformation gradient is multiplicatively decomposed into its active and passive parts, and this idea was the foundation of an active-strain approach based models. This approach was followed by D. Ambrosi et al. [21] (2011) and F. Nobile et al. [22] (2011), where a coupled model of cardiac tissues was presented, in which there were simulations in one-dimensional and two-dimensional geometry. In 2012, L. Mesin [25] followed the same idea initiated by C. Cherubini et al. [13], where he investigated the effect of electrical and mechanical activities of the myocardium on the dynamics of the spiral waves. All of the mentioned papers modeled the cardiac tissue as an isotropic material, however; the work done has been extended to include the

anisotropic structure of the cardiac tissues (F. Nobile et al. [29] (2012) and S. Rossi et al. [28] (2012)). Lately in 2013, a work was done by A. Gizzi et al. [30], modeling the cardiac tissue as anisotropic, where the interaction of calcium ions with contraction was included, and a three-dimensional mathematical model was presented.

Whether the active-stress or active-strain approaches are preferable is still an open issue, so authors suggest to perform experiments that lead to this decision (R. Frotscher [35]). However, these approaches are not the only ones available in the literature, due to the complexity of the heart material, researches represent it in many different ways (M. Doyle et al. [19]). Recently, in 2014, S. Goktepe et al. [31] utilized the two approaches together allowing them to combine the advantages of these two methods. However, this paper presented a three-dimensional generalized Hill model and considered the cardiac tissue as a hyper-elastic anisotropic material. Later on (2015), this model has been used to investigate the effects of myocardial infraction on the electromechanically coupled behavior of the heart [32], where the myocardial infraction is one of the leading causes of heart failure.

Two specific goals are presented in this thesis. First we will derive the mathematical models of the cardiac mechanics using the two approaches found in the literature: active-strain and active-stress and couple it with the cardiac electrical activity to form the cardiac electromechanical coupled models. Second, we will investigate numerically these models using one dimensional simulations and compare the results.

This thesis is structured as follows. In chapter 2, the reader gets a quick overview of elasticity theory which is the foundation of the mechanical activity of the heart. Then in chapter 3, we will adjust this theory to the cardiac tissues and derive the mathematical models based on the two approaches: active-strain and active-stress. Chapter 4 introduces the electrophysiology of the cardiac tissues, and couple it with the mechanical models provided in the previous chapter. Chapter 5 presents a numerical study in one dimensional case to the cardiac electromechanical coupled models and offers a comparison at the end. Finally, chapter 6 is devoted to conclusions and future work.

## Chapter 2: Elasticity Theory

Contraction of the heart causes deformation. For simplicity, some of the researches assumed that the heart undergoes small deformation, and therefore they modeled it as a linear elastic material (H. Dierckx et al. [33]). However, the ventricular wall of the cardiac muscles exhibits a change of thickness up to 40 percent during contraction (L. Waldman et al. [3] and S. Rossi et al. [28]), hence we can conclude that the cardiac muscle undergoes large deformation. Thus, we will be addressing in this thesis large deformation elasticity theory which corresponds to non linear elastic materials.

There are two concepts of fundamental importance for large deformation elasticity theory, which are the stress and the strain. The stress represents the force acting within the material per unit area, while the strain represents the length change of the material. The theory of elasticity is then composed of a set of equations which uniquely describes the state of stress, strain and deformation at each point within the elastic deformable body. Our aim is to develop the basic equations of nonlinear elasticity theory, and in order to do that we first investigate the kinematics of material deformation.

### 2.1 Kinematic Relations

Kinematics deals with the movement of materials when a set of forces act on it. The initial state of the material, where forces are not applied, is referred as the undeformed state. Then after applying some forces, the material deforms and reaches an equilibrium state known as the deformed state. Since deformation is defined by the movement of material particles, a method for labelling the particles is required.

We will define originally each material particle,  $\mathbf{X}$ , by a set of rectangular cartesian coordinates,  $(X_1; X_2; X_3)$ , in the undeformed region (or reference region)  $\Omega_o$ . Then when the body moves and deforms due to applied loads, the particles reconfigure to  $\mathbf{x}$ , with coordinates  $(x_1; x_2; x_3)$ , reaching an equilibrium state (or current state) in region  $\Omega_t$ , (see Figure 2.1).

The displacement, or deformation vector  $\mathbf{u}$ , of a material particle is the

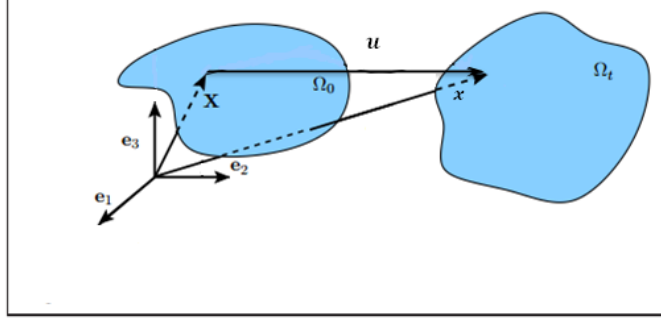


Figure 2.1: Motion from the reference configuration  $\Omega_0$  to the current configuration  $\Omega_t$

transition from the reference configuration to the current configuration. It is simply defined by the difference of the position vectors of a particle in both configurations:

$$\mathbf{u} = \mathbf{x} - \mathbf{X}. \quad (2.1)$$

Or in vector form:

$$\mathbf{u} = \begin{bmatrix} u_1 \\ u_2 \\ u_3 \end{bmatrix} = \begin{bmatrix} x_1 \\ x_2 \\ x_3 \end{bmatrix} - \begin{bmatrix} X_1 \\ X_2 \\ X_3 \end{bmatrix} = \begin{bmatrix} x_1 - X_1 \\ x_2 - X_2 \\ x_3 - X_3 \end{bmatrix}. \quad (2.2)$$

This displacement vector tells us when deformation happens how a point moves from the reference to the deformed configuration. However, we would also like to know how a small piece of material behaves as a result of this deformation. Intuitively, we expect deformation to consist of a combination of rotation and stretching notions that we shall discuss using tensors in what follows.

Consider a line element  $d\mathbf{X}$  coming out from position  $\mathbf{X}$  in the reference configuration (undeformed region) which becomes  $d\mathbf{x}$  in the current configuration (deformed region), then using notations of J. Humphrey et al. [8] we have the following relation:

$$d\mathbf{x} = \frac{\partial \mathbf{x}}{\partial \mathbf{X}} d\mathbf{X}. \quad (2.3)$$

Then we introduce the **deformation gradient tensor**  $\mathbf{F}$ . It is the central ingredient needed for describing the deformation of an entire neighborhood of a

particle. This tensor maps line elements in the reference configuration  $d\mathbf{X}$  into line elements in the deformed configuration  $d\mathbf{x}$  in the following relation:

$$d\mathbf{x} = \mathbf{F}d\mathbf{X}. \quad (2.4)$$

Then using equation (2.3) the deformation gradient tensor will be given by:

$$\mathbf{F} = \frac{\partial \mathbf{x}}{\partial \mathbf{X}} = \nabla_{\mathbf{x}}. \quad (2.5)$$

Or in matrix form:

$$\mathbf{F} = \begin{bmatrix} \frac{\partial x_1}{\partial X_1} & \frac{\partial x_1}{\partial X_2} & \frac{\partial x_1}{\partial X_3} \\ \frac{\partial x_2}{\partial X_1} & \frac{\partial x_2}{\partial X_2} & \frac{\partial x_2}{\partial X_3} \\ \frac{\partial x_3}{\partial X_1} & \frac{\partial x_3}{\partial X_2} & \frac{\partial x_3}{\partial X_3} \end{bmatrix}. \quad (2.6)$$

We need to introduce also the **inverse of the deformation gradient tensor**  $\mathbf{F}^{-1}$ , which represents the transformation from the current configuration to the reference configuration, and written as in [8] by:

$$\mathbf{F}^{-1} = \frac{\partial \mathbf{X}}{\partial \mathbf{x}}. \quad (2.7)$$

Or in matrix form using notations by A. Fortin and A. Garon [36]:

$$\mathbf{F}^{-1} = \begin{bmatrix} \frac{\partial X_1}{\partial x_1} & \frac{\partial X_1}{\partial x_2} & \frac{\partial X_1}{\partial x_3} \\ \frac{\partial X_2}{\partial x_1} & \frac{\partial X_2}{\partial x_2} & \frac{\partial X_2}{\partial x_3} \\ \frac{\partial X_3}{\partial x_1} & \frac{\partial X_3}{\partial x_2} & \frac{\partial X_3}{\partial x_3} \end{bmatrix}, \quad (2.8)$$

where  $\mathbf{F}\mathbf{F}^{-1} = \mathbf{F}^{-1}\mathbf{F} = \mathbf{I}$ .

Now we explore the relationship between the displacement, deformation gradient tensor, and inverse of deformation gradient tensor. Rearranging equation

(2.1):

$$\mathbf{x} = \mathbf{X} + \mathbf{u}. \quad (2.9)$$

Then using equations (2.5) and (2.7), we conclude the following:

$$\mathbf{F} = \mathbf{I} + \nabla_X \mathbf{u}, \quad (2.10)$$

$$\mathbf{F}^{-1} = \mathbf{I} - \nabla_x \mathbf{u}. \quad (2.11)$$

We examined that the deformation gradient tensor is responsible for the line element transformation between the reference and the current configurations; however, the Jacobian of the deformation  $J$  is responsible for the volume transformation. It is the measure of how the volume of a material element has changed with deformation, and for this reason it is often called the volume ratio. It is defined as the determinant of the deformation gradient tensor:

$$J = \det(\mathbf{F}). \quad (2.12)$$

For an incompressible material, one for which the volume change is zero, the relation  $J = \det(\mathbf{F}) = 1$  holds. The incompressibility constraint is therefore  $J - 1 = 0$ .

Another tensor important for large deformation is the **right Cauchy-Green strain tensor**  $\mathbf{C}$ . It gives direct information about deformation of the body, and measures how the length of the line elements and angles between line elements change between configurations. It is defined by:

$$\mathbf{C} = \mathbf{F}^T \mathbf{F}. \quad (2.13)$$

Whereas the right Cauchy-Green strain tensor gives information about rotation and stretch of line elements, the **Green-Lagrange strain tensor**  $\mathbf{E}$  gives information about the change in the squared length of elements, defined by:

$$\mathbf{E} = \frac{1}{2}(\mathbf{C} - \mathbf{I}) = \frac{1}{2}(\mathbf{F}^T \mathbf{F} - \mathbf{I}). \quad (2.14)$$

After introducing some basic tensors, we are interested in relating them to the material and this can be done using **Strain Energy Density  $\mathbf{W}$**  which is the measure of how much energy is stored in small volume elements in the body due to deformation. It can be written in terms of the deformation gradient tensor, or Cauchy-Green strain tensor, or strain tensor as:

$$\mathbf{W} = \mathbf{W}(\mathbf{E}) = \mathbf{W}(\mathbf{C}) = \mathbf{W}(\mathbf{F}). \quad (2.15)$$

Based on experimental observations of the material, the strain energy density changes. For instance, certain types of rubber exhibit almost isotropic behaviour and can be referred to Mooney-Rivlin materials. For this isotropic material the strain energy density  $\mathbf{W}$  is given by:

$$\mathbf{W} = c_1(I_1 - 3) + c_2(I_2 - 3), \quad (2.16)$$

where  $c_1$  and  $c_2$  are material constants (mechanical properties) which must be estimated experimentally,  $I_1$  and  $I_2$  are invariants of the right Cauchy-Green strain tensor  $\mathbf{C}$  given by:

$$I_1 = \text{tr}\mathbf{C} = \text{tr}(\mathbf{F}^T\mathbf{F}), \quad (2.17)$$

$$I_2 = \frac{1}{2}[(\text{tr}\mathbf{C})^2 - \text{tr}\mathbf{C}^2]. \quad (2.18)$$

A subset of the Mooney-Rivlin materials are the Neo-Hookean materials, which are characterised by setting  $c_2 = 0$  in equation (2.16):

$$\mathbf{W} = c_1(I_1 - 3). \quad (2.19)$$

To ensure the incompressibility constraint  $J - 1 = 0$  at each point of the tissue of a material by preserving the volume, a pressure function  $p$ , known as Lagrange Multiplier can be introduced, then the strain energy function  $\mathbf{W}$  will be written in the form:

$$\mathbf{W} = \mathbf{W}(\mathbf{F}) - p(J - 1). \quad (2.20)$$

There are much more forms for the strain energy density, other than Mooney-Rivlin and Neo-Hookean, available in the literature (see [7], [19], [30]), depending on the type of the material.

After establishing the kinematic framework for large deformation analysis, we are now interested in the governing force and equilibrium equations, which will be presented in the next section.

## 2.2 Stress Equilibrium

Equilibrium equations that consider deformed material follow from Newton's law of motion where in the absence of body forces, the equation of motion can read:

$$\nabla_x \cdot \boldsymbol{\sigma} = 0. \quad (2.21)$$

Or it can be written in matrix form as:

$$\nabla_x \cdot \boldsymbol{\sigma} = \begin{bmatrix} \frac{\partial \sigma_{11}}{\partial x_1} + \frac{\partial \sigma_{12}}{\partial x_2} + \frac{\partial \sigma_{13}}{\partial x_3} \\ \frac{\partial \sigma_{21}}{\partial x_1} + \frac{\partial \sigma_{22}}{\partial x_2} + \frac{\partial \sigma_{23}}{\partial x_3} \\ \frac{\partial \sigma_{31}}{\partial x_1} + \frac{\partial \sigma_{32}}{\partial x_2} + \frac{\partial \sigma_{33}}{\partial x_3} \end{bmatrix} = \begin{bmatrix} 0 \\ 0 \\ 0 \end{bmatrix}, \quad (2.22)$$

where  $\boldsymbol{\sigma}$  is called the **Cauchy stress tensor**, and it represents the forces in the deformed configuration per unit area in the deformed configuration, defined by:

$$\boldsymbol{\sigma} = \frac{d\mathbf{f}}{d\mathbf{a}},$$

$d\mathbf{f}$  is a true force applied to a current area element  $d\mathbf{a}$  in the deformed region.

Since it is difficult to find the stresses in the deformed region, it will be convenient to transform the above equation to the undeformed region. This can be done using Nanson's relation [1]:

$$d\mathbf{a} = J\mathbf{F}^{-T}d\mathbf{A},$$

where  $d\mathbf{a}$  is a current area element (in the deformed configuration), and  $d\mathbf{A}$  is a

reference area element (in the undeformed configuration).

The Cauchy stress tensor  $\boldsymbol{\sigma} = \frac{d\mathbf{f}}{d\mathbf{a}}$ , then the stress in the undeformed region reads:

$$\frac{d\mathbf{f}}{d\mathbf{A}} = \boldsymbol{\sigma} J \mathbf{F}^{-T}.$$

But this value constitute the actual force applied to an area of element in the reference configuration, and it is represented by the **first Piola-Kirchhoff stress tensor  $\mathbf{P}$** :

$$\mathbf{P} = \frac{d\mathbf{f}}{d\mathbf{A}}.$$

Thus, the first Piola-Kirchhoff stress tensor will be:

$$\mathbf{P} = \boldsymbol{\sigma} J \mathbf{F}^{-T}. \quad (2.23)$$

Rewriting the equation of motion (2.21) in the reference area, using Nanson's relation, we get:

$$\nabla_x \cdot \boldsymbol{\sigma} = \nabla_X \cdot (\boldsymbol{\sigma} J \mathbf{F}^{-T}) = \nabla_X \cdot \mathbf{P} = 0. \quad (2.24)$$

Thus the equilibrium equation simply reads:

$$\nabla_X \cdot \mathbf{P} = 0, \quad (2.25)$$

where  $\mathbf{P}$  can be derived using the strain energy density  $\mathbf{W}$  that depends on the type of the material:

$$\mathbf{P} = \frac{\partial \mathbf{W}}{\partial \mathbf{F}}, \quad (2.26)$$

or for incompressible materials, it will read as:

$$\mathbf{P} = \frac{\partial \mathbf{W}}{\partial \mathbf{F}} - J p \mathbf{F}^{-T}. \quad (2.27)$$

The material representation can be also considered independent of body motion. In this case, the first Piola-Kirchhoff stress tensor can be written as:

$$\mathbf{P} = \mathbf{F}\mathbf{T}, \quad (2.28)$$

where  $\mathbf{T}$  is the **second Piola-Kirchhoff stress tensor**, which relates the forces in the undeformed configuration with areas in the undeformed configuration.

Therefore, the governing equilibrium equation (2.25) will read:

$$\nabla_X \cdot (\mathbf{F}\mathbf{T}) = 0. \quad (2.29)$$

Here we addressed the mechanics for any material in general. Now our aim is to discuss the mechanics that correspond to the cardiac in specific. Equations (2.25) and (2.29) will be considered for the cardiac mechanical modelling depending on the approaches we will be explaining in the next chapter.

## Chapter 3: Cardiac Mechanics

The cardiac tissues can be regarded as an inhomogeneous, anisotropic (filled with fluid), and incompressible or nearly compressible elastic material (see G. Holzapfel and R. Ogden [15]). This tissue is subject to external load forming a deformation. We are interested in two main approaches addressing the mechanics of these tissues that we found in the literature, which are the active-strain approach [6] and the active-stress approach [13].

### 3.1 Active-Strain Approach

We consider the heart as a hyper-elastic body subject to external load. Following [13], active-strain approach, the deformation gradient tensor is multiplicatively decomposed into two factors, the micro (active,  $\mathbf{F}_o$ ) and the macro (passive,  $\mathbf{F}_e$ ):

$$\mathbf{F} = \mathbf{F}_e \mathbf{F}_o, \quad (3.1)$$

note that  $\mathbf{F}_o$  corresponds to the fibers while  $\mathbf{F}_e$  corresponds to the material.

Simply it is assumed that at any point  $\mathbf{X}$  the fibers are oriented according to one direction only, namely,  $\mathbf{n}$ . The microscale part of the deformation tensor can take the form:

$$\mathbf{F}_o = 1 + \gamma(V)\mathbf{n} \otimes \mathbf{n}, \quad (3.2)$$

where  $V$  is the electric potential. The function  $\gamma$  corresponds to the contraction of the cardiac muscle depending on the value of the potential.

In this thesis, we restrict ourselves to the simple rule [21]:

$$\gamma = -\beta V. \quad (3.3)$$

Muscle contraction involves a 30 percent strain [21], and therefore we choose the parameter  $\beta$  to be 0.3. According to the simple rule (3.3),  $\gamma > 0$  denotes elongation, and  $\gamma < 0$  denotes contraction. Take as a remark that the determinant of microscale part of the deformation tensor is:

$$\det(\mathbf{F}_o) = 1 + \gamma. \quad (3.4)$$

Moreover, it is assumed that the strain energy of the cardiac muscle depends only on the deformation at the macroscale:

$$\mathbf{W} = \mathbf{W}(\mathbf{F}_e). \quad (3.5)$$

For simplicity an isotropic Neo-Hookean material is considered and therefore the strain energy is considered as:

$$\mathbf{W} = c_1(I_1 - 3), \quad (3.6)$$

where  $I_1$  is the first invariant of the left Cauchy-Green tensor of  $\mathbf{F}_e$ :

$$I_1 = \text{tr}(\mathbf{F}_e^T \mathbf{F}_e) = \mathbf{F}_e \cdot \mathbf{F}_e. \quad (3.7)$$

The corresponding Piola-Kirchhoff stress tensor is given by:

$$\mathbf{P} = J_o \frac{\partial \mathbf{W}}{\partial \mathbf{F}_e} \mathbf{F}_o^{-T}, \quad (3.8)$$

where  $J_o = \det(\mathbf{F}_o)$ .

Since the cardiac tissue is modeled here as an incompressible material, the first Piola-Kirchhoff stress tensor will take the form:

$$\mathbf{P} = J_o \frac{\partial \mathbf{W}}{\partial \mathbf{F}_e} \mathbf{F}_o^{-T} - Jp \mathbf{F}^{-T}. \quad (3.9)$$

To write this equation in terms of the displacement  $\mathbf{u}$  some derivations will be done as follows:

$$\mathbf{P} = J_o \frac{\partial \mathbf{W}}{\partial I_1} \frac{\partial I_1}{\partial \mathbf{F}_e} \mathbf{F}_o^{-T} - Jp \mathbf{F}^{-T},$$

but  $\frac{\partial \mathbf{W}}{\partial I_1} = c_1$  and  $\frac{\partial I_1}{\partial \mathbf{F}_e} = 2\mathbf{F}_e$ , then:

$$\mathbf{P} = 2c_1 J_o \mathbf{F}_e \mathbf{F}_o^{-T} - Jp \mathbf{F}^{-T},$$

by letting  $\mu = 2c_1$ , we get:

$$\mathbf{P} = \mu J_o \mathbf{F}_e \mathbf{F}_o^{-T} - Jp \mathbf{F}^{-T},$$

but  $\mathbf{F}_e = \mathbf{F} \mathbf{F}_o^{-1}$  using equation (3.1) implies:

$$\mathbf{P} = \mu J_o \mathbf{F} \mathbf{F}_o^{-1} \mathbf{F}_o^{-T} - Jp \mathbf{F}^{-T}.$$

After substituting the value of the deformation gradient using (2.10) in the above equation, the first Piola-Kirchhoff stress tensor will be:

$$\mathbf{P} = \mu J_o (\mathbf{I} + \nabla_X \mathbf{u}) \mathbf{F}_o^{-1} \mathbf{F}_o^{-T} - Jp (\mathbf{I} + \nabla_X \mathbf{u})^{-T}. \quad (3.10)$$

Finally the equation of equilibrium (2.25) will read:

$$\nabla_X \cdot (\mu J_o (\mathbf{I} + \nabla_X \mathbf{u}) \mathbf{F}_o^{-1} \mathbf{F}_o^{-T} - Jp (\mathbf{I} + \nabla_X \mathbf{u})^{-T}) = 0. \quad (3.11)$$

This is the governing mechanical equation that corresponds to the active-strain approach.

## 3.2 Active-Stress Approach

Another approach was initiated by P. Hunter et al. [6], where mechanical stresses in tissues are modeled as the summation of a passive and an active stress component, the second Piola-Kirchhoff stress tensor is given by:

$$\mathbf{T} = \mathbf{T}_P + \mathbf{T}_A. \quad (3.12)$$

The passive part of this tensor depends on the material properties, which is represented by the strain energy density function  $\mathbf{W}$ , and is given by:

$$\mathbf{T}_P = 2 \frac{\partial \mathbf{W}}{\partial \mathbf{C}}.$$

While the active part depends on an active tension component  $T_a$ , given

by:

$$\mathbf{T}_A = T_a \mathbf{C}^{-1}.$$

The active tension  $T_a$  provides a phenomenological description of the tension within cardiac tissue. It is determined using a voltage generated by the electrical system and it is used to couple the electrical and mechanical models.

After substituting these values in equation (3.12), the second Piola-Kirchhoff stress tensor will be:

$$\mathbf{T} = 2 \frac{\partial \mathbf{W}}{\partial \mathbf{C}} + T_a \mathbf{C}^{-1}. \quad (3.13)$$

Using the strain energy density function for the Mooney-Rivlin material provided by equation (2.16):

$$\mathbf{W} = c_1(I_1 - 3) + c_2(I_2 - 3), \quad (3.14)$$

with  $I_1$  and  $I_2$  as the first two principal invariants of  $\mathbf{C}$  given by equations (2.17) and (2.18).

We need to find the value of the second Piola-Kirchhoff stress tensor adjusted to this approach from which we can get the first Piola-Kirchhoff stress tensor, and then we will be able to find the equilibrium equation.

We start by finding the value of  $\frac{\partial \mathbf{W}}{\partial \mathbf{C}}$  and substitute it in (3.12)

$$\frac{\partial \mathbf{W}}{\partial \mathbf{C}} = \frac{\partial \mathbf{W}}{\partial I_1} \frac{\partial I_1}{\partial \mathbf{C}} + \frac{\partial \mathbf{W}}{\partial I_2} \frac{\partial I_2}{\partial \mathbf{C}}, \quad (3.15)$$

where  $\frac{\partial \mathbf{W}}{\partial I_1} = c_1$  and  $\frac{\partial \mathbf{W}}{\partial I_2} = c_2$  using equation (3.14), also  $\frac{\partial I_1}{\partial \mathbf{C}} = \mathbf{I}$  and  $\frac{\partial I_2}{\partial \mathbf{C}} = tr(\mathbf{C})\mathbf{I} - \mathbf{C}$  using equations (2.17) and (2.18).

Substitute all these values in the previous equation we get:

$$\frac{\partial \mathbf{W}}{\partial \mathbf{C}} = c_1 \mathbf{I} + c_2((tr \mathbf{C})\mathbf{I} - \mathbf{C}). \quad (3.16)$$

Thus the second Piola-Kirchhoff stress tensor given in (3.13) will be:

$$\mathbf{T} = (2c_1 + 2c_2 tr \mathbf{C})\mathbf{I} - 2c_2 \mathbf{C} + T_a \mathbf{C}^{-1}. \quad (3.17)$$

Using equation (3.8), the first Piola-Kirchhoff stress tensor will be:

$$\mathbf{P} = (2c_1 + 2c_2 \text{tr} \mathbf{C}) \mathbf{F} - 2c_2 \mathbf{F} \mathbf{C} + T_a \mathbf{F} \mathbf{C}^{-1}. \quad (3.18)$$

Therefore the equilibrium equation (2.25) will read:

$$\nabla_X \cdot ((2c_1 + 2c_2 \text{tr} \mathbf{C}) \mathbf{F} - 2c_2 \mathbf{F} \mathbf{C} + T_a \mathbf{F} \mathbf{C}^{-1}) = 0. \quad (3.19)$$

This is the governing mechanical equation that corresponds to the active-stress approach.

## Chapter 4: Cardiac Electromechanics

After deriving the mechanical equations that correspond to the two approaches, we are interested in the electrical activity of the cardiac tissues and its governing equations. Finally, we will couple the electrical and the mechanical equations to form models that correspond to the two approaches.

### 4.1 Cardiac Electrophysiology

Cardiac electrophysiology is usually modeled by two classes: bidomain and monodomain. The book by J. Keener and J. Sneyd [5] is an excellent description in this respect. The first class called the bidomain model, proposed in 1978 by L. Tung and D. Geselowitz, is a system of two nonlinear partial differential equations coupled with one ordinary differential equation. This model gives an accurate representation of the electrophysiological wave in the cardiac tissues; however, it is computationally expensive. The bidomain model can be reduced to a monodomain model, which is the second class of electrophysiological representation. The monodomain model consists of a single nonlinear partial differential equation for the transmembrane potential coupled with the same equation of ordinary differential equation for the recovery variable, and it describes the dynamics of a general excitable cardiac tissue. Its equations take the form:

$$\frac{\partial V}{\partial t} = \nabla \cdot (\mathbf{D} \nabla V) + f, \quad (4.1)$$

$$\frac{\partial w}{\partial t} = g, \quad (4.2)$$

where  $V$  is the transmembrane potential,  $w$  is the recovery variable,  $\mathbf{D}$  is a diffusion tensor, and both  $f$  and  $g$  are functions depending on the ionic model.

There are many representations for the functions  $f$  and  $g$ ; however, we restrict our attention to the simplified two-variable model called Aliev-Panfilov [4], where the two functions  $f$  and  $g$  have the form:

$$f(V, w) = -kV(V - \alpha)(V - 1) - Vw,$$

$$g(V, w) = \left( \epsilon + \frac{\mu_1 w}{\mu_2 + V} \right) (-w - kV(V - \alpha - 1)).$$

Thus the Aliev-Panfilov monodomain model will read:

$$\frac{\partial V}{\partial t} = \nabla \cdot (\mathbf{D} \nabla V) - kV(V - \alpha)(V - 1) - Vw, \quad (4.3)$$

$$\frac{\partial w}{\partial t} = \left( \epsilon + \frac{\mu_1 w}{\mu_2 + V} \right) (-w - kV(V - \alpha - 1)), \quad (4.4)$$

where  $\mu_1$ ,  $\mu_2$ ,  $\alpha$ ,  $\epsilon$ , and  $k$  are parameters used to modify the behavior of the wave based on observations [4]. Now these equations (4.3) and (4.4) should be coupled with the mechanical models presented previously.

## 4.2 Cardiac Electromechanical Coupling

In order to couple the electrical equations with the mechanical equations derived in the previous sections, we have to follow the two approaches mentioned before: active-strain approach and active-stress approach.

**4.2.1. Active-strain approach.** First, following the active-strain approach (see work done in [21]), the electrical equations (4.3) and (4.4) in a material frame of reference after the mechanics is applied rewrites as:

$$\frac{\partial}{\partial t}(JV) = \nabla_X \cdot (J\mathbf{F}^{-1}\mathbf{D}\mathbf{F}^{-T}\nabla V) - kJV(V - \alpha)(V - 1) - JVw, \quad (4.5)$$

$$\frac{\partial}{\partial t}(Jw) = J \left( \epsilon + \frac{\mu_1 w}{\mu_2 + V} \right) (-w - kV(V - \alpha - 1)). \quad (4.6)$$

Thus the general electromechanical cardiac coupled model reads:

$$\left\{ \begin{array}{l} \frac{\partial}{\partial t}(JV) = \nabla_X \cdot (J\mathbf{F}^{-1}\mathbf{D}\mathbf{F}^{-T}\nabla V) - kJV(V - \alpha)(V - 1) - JVw, \\ \frac{\partial}{\partial t}(Jw) = J \left( \epsilon + \frac{\mu_1 w}{\mu_2 + V} \right) (-w - kV(V - \alpha - 1)), \\ \nabla_X \cdot (\mu J_o(\mathbf{I} + \nabla_X \mathbf{u})\mathbf{F}_o^{-1}\mathbf{F}_o^{-T} - Jp(\mathbf{I} + \nabla_X \mathbf{u})^{-T}) = 0. \end{array} \right. \quad (4.7)$$

This model includes the microscopic structure of the cardiac tissues since it dictates the fibers and includes them in the equations, and is considered as the final set of equations for the active-strain approach that will be used in the numerical simulations later.

**4.2.2. Active-stress approach.** Next, following the active-stress approach (see work done in [9]), where isotropic material properties has been assumed, and anisotropic behaviour [6] have been neglected for simplicity. The general electromechanical cardiac coupled model reads:

$$\left\{ \begin{array}{l} \frac{\partial V}{\partial t} = \nabla \cdot (\mathbf{D} \nabla V) - kV(V - \alpha)(V - 1) - Vw - I_g, \\ \frac{\partial w}{\partial t} = \left( \epsilon + \frac{\mu_1 w}{\mu_2 + V} \right) (-w - kV(V - \alpha - 1)), \\ \frac{\partial T_a}{\partial t} = \epsilon(V)(K_{T_a} V - T_a), \\ \nabla_X \cdot ((2c_1 + 2c_2 \text{tr} \mathbf{C})) \mathbf{F} - 2c_2 \mathbf{F} \mathbf{C} + T_a \mathbf{F} \mathbf{C}^{-1} = 0, \end{array} \right. \quad (4.8)$$

where  $\mathbf{D}$  is the diffusion constant, and  $I_g$  is the stretch-activated current.

The main difference from the previous approach is that they introduced the active tension  $T_a$  to their equations, with the rate of change given by:

$$\frac{\partial T_a}{\partial t} = \epsilon(V)(K_{T_a} V - T_a), \quad (4.9)$$

where  $K_{T_a}$  is a parameter that controls the amplitude of  $T_a$ ,  $V$  is the transmembrane potential, and  $T_a$  increases with  $V$  with a delay fixed by  $\epsilon(V)$ :

$$\epsilon(V) = \begin{cases} 0.1, & \text{if } V > a \\ 1, & \text{if } V \leq a \end{cases}.$$

System (4.8) is the final set of equations for the active-stress approach that will be used in the numerical simulations later.

## Chapter 5: Numerical Simulations

In this section, we specify the general model of electromechanical coupling described in the previous chapter using the two approaches to one dimensional geometry, and we illustrate the numerical method applied to obtain the numerical approximations of the solution. We will simplify equations (4.7) and (4.8) to one dimension.

### 5.1 One Dimensional Active-Strain Approach

In one spatial dimension, following D. Ambrosi et al. [21], the active deformation tensor  $\mathbf{F}_o$ , using equation (3.2), simply reads:

$$F_o = 1 + \gamma. \quad (5.1)$$

By assuming one-dimensional motion, the momentum equation (3.11) reads:

$$\left( \frac{x'}{1 + \gamma} \right)' = 0, \quad (5.2)$$

which can be immediately integrated (see work done in [21]) to give:

$$x' = 1 + \gamma, \quad (5.3)$$

this work will be recalled as method method.

We start by assuming that  $\gamma(V)$  is a smooth function:

$$\gamma = -\beta V.$$

Using the first two equations of the system (4.7) and equation (5.3), we get the final problem of electromechanical coupling:

$$\left\{ \begin{array}{l} \frac{\partial}{\partial t}((1 - \beta V)V) = \mathbf{D} \frac{\partial}{\partial X} \left( \frac{1}{1 - \beta V} \frac{\partial V}{\partial X} \right) - k(1 - \beta V)V(V - \alpha)(V - 1) - \\ (1 - \beta V)Vw, \\ \frac{\partial}{\partial t}((1 - \beta V)w) = (1 - \beta V) \left( \epsilon + \frac{\mu_1 w}{\mu_2 + V} \right) (-w - kV(V - \alpha - 1)), \\ \frac{\partial x}{\partial X} = 1 - \beta V. \end{array} \right. \quad (5.4)$$

We can simplify the system by dividing the first two equations by the term  $(1 - \beta V)$  getting:

$$\left\{ \begin{array}{l} \frac{\partial V}{\partial t} = \frac{\mathbf{D}}{(1 - \beta V)^2} \frac{\partial^2 V}{\partial X^2} - kV(V - \alpha)(V - 1) - Vw, \\ \frac{\partial w}{\partial t} = \left( \epsilon + \frac{\mu_1 w}{\mu_2 + V} \right) (-w - kV(V - \alpha - 1)), \\ \frac{\partial x}{\partial X} = 1 - \beta V. \end{array} \right. \quad (5.5)$$

This is the one-dimensional Panfilov model that we are going to use following the active-strain approach. We will start by approximating the derivatives with a semi implicit finite difference method. Replacing the partial derivatives  $\frac{\partial V}{\partial t}$ ,  $\frac{\partial w}{\partial t}$ , and  $\frac{\partial x}{\partial X}$  with forward difference equation:

$$\frac{\partial V_i}{\partial t} = \frac{V_i^{n+1} - V_i^n}{\Delta t}, \quad (5.6)$$

$$\frac{\partial w_i}{\partial t} = \frac{w_i^{n+1} - w_i^n}{\Delta t}, \quad (5.7)$$

$$\frac{\partial x}{\partial X} = \frac{x_{i+1}^{n+1} - x_i^{n+1}}{\Delta X}. \quad (5.8)$$

And the second order partial differential equation  $\frac{\partial^2 V}{\partial X^2}$  with the second order central difference equation:

$$\frac{\partial^2 V^{n+1}}{\partial X^2} = \frac{V_{i+1}^{n+1} - 2V_i^{n+1} + V_{i-1}^{n+1}}{\Delta X^2}, \quad (5.9)$$

where  $i$  represents the position,  $n$  represents the time step,  $\Delta X$  is the spacial step size,  $\Delta t$  is the time step size,  $0 \leq t \leq T$ ,  $0 \leq X \leq L$ ,  $N$  is the number of time steps, and  $M$  is the number of space steps:

$$\Delta t = \frac{T}{N}, \Delta X = \frac{L}{M}$$

Replace equations (5.6), (5.7), and (5.9) in the system (5.5), we obtain:

$$\left\{ \begin{array}{l} \frac{V_i^{n+1} - V_i^n}{\Delta t} = \frac{\mathbf{D}}{(1 - \beta V_i^n)^2} \left( \frac{V_{i+1}^{n+1} - 2V_i^{n+1} + V_{i-1}^{n+1}}{\Delta X^2} \right) - \\ kV_i^n(V_i^n - \alpha)(V_i^n - 1) - V_i^n w_i^n, \\ \frac{w_i^{n+1} - w_i^n}{\Delta t} = \left( \epsilon + \frac{\mu_1 w_i^n}{\mu_2 + V_i^n} \right) (-w_i^n - kV_i^n(V_i^n - \alpha - 1)), \\ \frac{x_{i+1}^{n+1} - x_i^{n+1}}{\Delta X} = 1 - \beta V_i^{n+1}. \end{array} \right. \quad (5.10)$$

To rearrange these equations easily we let the following:

$$r = \frac{\Delta t}{\Delta X^2},$$

$$f_i^n = -kV_i^n(V_i^n - \alpha)(V_i^n - 1) - V_i^n w_i^n,$$

$$g_i^n = \left( \epsilon + \frac{\mu_1 w_i^n}{\mu_2 + V_i^n} \right) (-w_i^n - kV_i^n(V_i^n - \alpha - 1)).$$

Then equations in (5.10) become:

$$\left( \frac{-\mathbf{D}r}{(1 - \beta V_i^n)^2} \right) V_{i-1}^{n+1} + \left( 1 + \frac{2\mathbf{D}r}{(1 - \beta V_i^n)^2} \right) V_i^{n+1} + \left( \frac{-\mathbf{D}r}{(1 - \beta V_i^n)^2} \right) V_{i+1}^{n+1} = \\ V_i^n + \Delta t f_i^n, \quad (5.11)$$

$$w_i^{n+1} = w_i^n + \Delta t g_i^n, \quad (5.12)$$

$$x_{i+1}^{n+1} = x_i^{n+1} + \Delta X(1 - \beta V_i^{n+1}). \quad (5.13)$$

Equations (5.12) and (5.13) will be solved explicitly. On the other hand, equation (5.11) will be written in matrix form  $\mathbf{A}\mathbf{v} = \mathbf{b}$ , then solved to get  $\mathbf{v}$  (unknown potential vector) using LU decomposition method implemented in matlab. The above numerical scheme has a second order accuracy in space and a first order accuracy in time; however, higher order methods can be used to avoid numerical instabilities, but we limit ourselves to first order accuracy in time since time discretization is not our goal in this thesis. Numerical simulations require values at the boundaries to obtain a solution. Since we have a second order of accuracy we used a second order Neumann boundary conditions.

For  $i = 1$ , we use forward difference approximation:

$$\frac{-3V_1^{n+1} + 4V_2^{n+1} - V_3^{n+1}}{2\Delta X} = 0.$$

For  $i = M + 1$ , we use backward difference approximation:

$$\frac{V_{M-1}^{n+1} - 4V_M^{n+1} + 3V_{M+1}^{n+1}}{2\Delta X} = 0.$$

The matrix form  $\mathbf{A}\mathbf{v} = \mathbf{b}$  will read:

$$\begin{bmatrix} -3 & 4 & -1 & 0 & \dots & 0 \\ -r & (1+2r) & -r & 0 & \dots & 0 \\ 0 & \ddots & \ddots & \ddots & \ddots & \vdots \\ 0 & \dots & 0 & -r & (1+2r) & -r \\ 0 & \dots & 0 & 1 & -4 & 3 \end{bmatrix} \begin{bmatrix} V_1^{n+1} \\ \vdots \\ \vdots \\ \vdots \\ V_{M+1}^{n+1} \end{bmatrix} = \begin{bmatrix} 0 \\ V_2^n + \Delta t f_2^n \\ \vdots \\ V_M^n + \Delta t f_M^n \\ 0 \end{bmatrix}.$$

We start with an initial condition:

$$v(X, 0) = \begin{cases} 1, & \text{if } X \leq 30 \\ 0, & \text{if } X > 30 \end{cases}, w(X, 0) = 0.$$

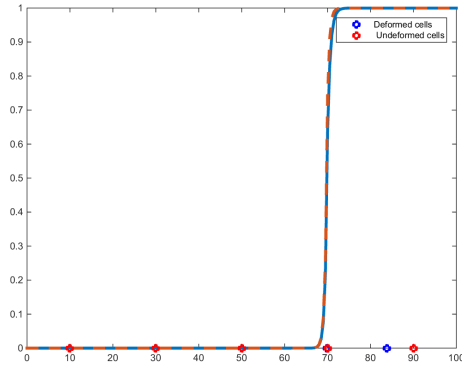
Then we solve the system of equations and find  $\mathbf{v}$ . The vector  $\mathbf{v}$  is now filled with the new  $V_i^{n+1}$ , where  $n$  represents the current time step of the solution, and hence we can go to the next time step. Note that  $\Delta X$  and  $\Delta t$  are constants, so matrix  $\mathbf{A}$  doesn't change with time (we computed only once), while vectors  $\mathbf{v}$ ,  $\mathbf{b}$  need to be recomputed at each time step. This is repeated until we reach the end of the time interval that is to be studied.

First we validate our scheme by using the following analytical solution:  $V = e^{-x^2}$ ,  $w = 3e^{-x^2}$  and we get the expected order of the scheme.

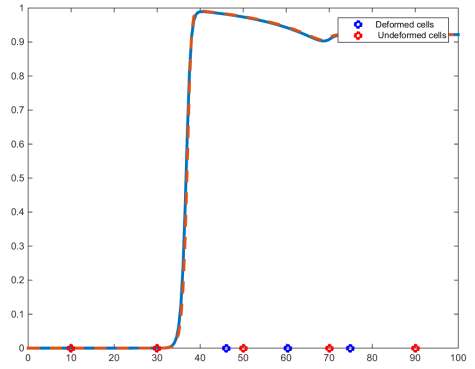
For the electromechanical model the physical parameters used are fixed according to values taken from the literature [9], given by:

parameter	$k$	$\alpha$	$\epsilon$	$\mu_1$	$\mu_2$	$D$
value	8	0.1	0.01	0.12	0.3	1

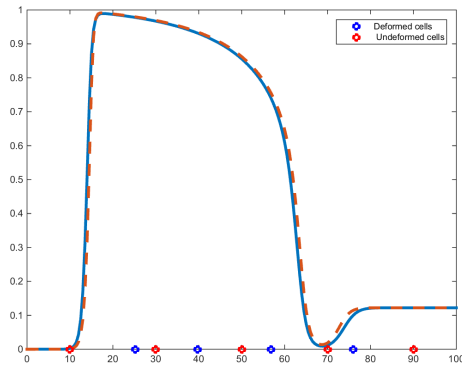
The numerical result is presented in Figure 5.1. This figure displays a sequence of time evolution of action potential  $V$ , where the dashed line corresponds to the action potential before mechanics is applied and the solid line is the action potential after mechanics is applied. To check the effect of the electromechanical coupling in the one dimensional simulation, we will fix some nodes (red dots color) on the computational domain and we observe how these nodes will deform as the electrical wave is moving. As can be seen in Figure 5.1 as the electrical wave propagates through the fiber we will notice the forward movement of the nodes (blue dots color), and once it passes away the nodes come back to their initial position. As a consequence, this mechanical activity has an effect on the electrical wave since the dashed line did not coincide with the solid line.



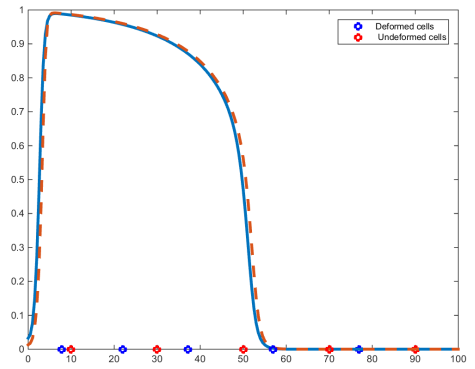
a)  $t = 0.2$



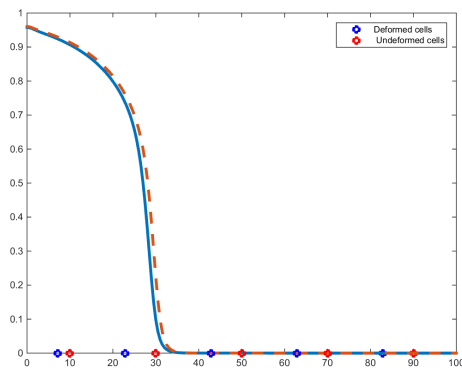
b)  $t = 23.8$



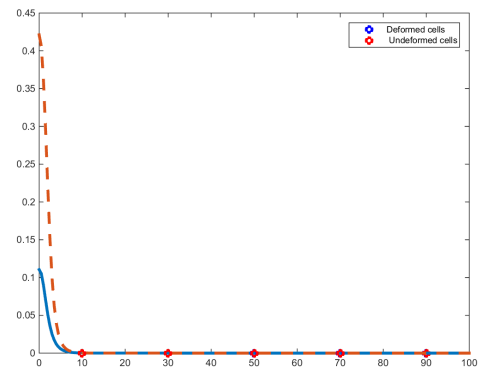
c)  $t = 39.8$



d)  $t = 47.8$



e)  $t = 63.8$



f)  $t = 83.8$

Figure 5.1: Deformation corresponding to active-strain approach: Numerical method 1

We found that the behavior of the nodes shown in Figure 5.1 is not realistic and can be linked only to numerical approach. For this reason we propose a way different than that in [21], recall it method 2. We write equation (5.2):

$$\left(\frac{x'}{1+\gamma}\right)' = 0,$$

as follows:

$$\frac{x''}{1+\gamma} - \frac{x'\gamma'}{(1+\gamma)^2} = 0. \quad (5.14)$$

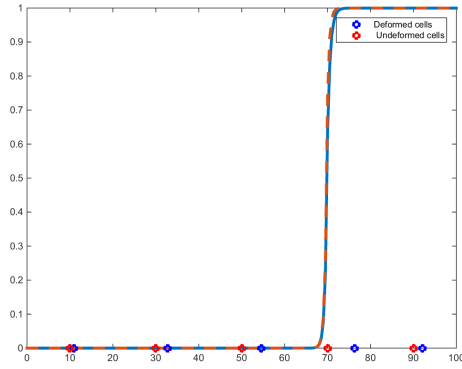
Then the electromechanical coupled model will read as:

$$\begin{cases} \frac{\partial V}{\partial t} = \frac{\mathbf{D}}{(1-\beta V)^2} \frac{\partial^2 V}{\partial X^2} - kV(V-\alpha)(V-1) - Vw, \\ \frac{\partial w}{\partial t} = \left(\epsilon + \frac{\mu_1 w}{\mu_2 + V}\right) (-w - kV(V-\alpha-1)), \\ \frac{1}{(1-\beta V)} \frac{\partial^2 x}{\partial X^2} + \beta \frac{1}{(1-\beta V)^2} \frac{\partial x}{\partial X} \frac{\partial V}{\partial X} = 0. \end{cases} \quad (5.15)$$

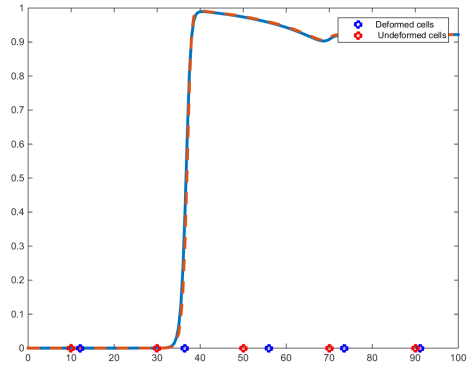
By approximating the derivatives with a semi implicit finite difference method, model (5.15) will read:

$$\begin{cases} \frac{V_i^{n+1} - V_i^n}{\Delta t} = \frac{\mathbf{D}(V_{i+1}^{n+1} - 2V_i^{n+1} + V_{i-1}^{n+1})}{(1-\beta V_i^n)^2 \Delta X^2} - kV_i^n(V_i^n - \alpha)(V_i^n - 1) - V_i^n w_i^n, \\ \frac{w_i^{n+1} - w_i^n}{\Delta t} = \left(\epsilon + \frac{\mu_1 w_i^n}{\mu_2 + V_i^n}\right) (-w_i^n - kV_i^n(V_i^n - \alpha - 1)), \\ \frac{(x_{i+1}^{n+1} - 2x_i^{n+1} + x_{i-1}^{n+1})}{(1-\beta V_i^n) \Delta X^2} + \beta \frac{1}{(1-\beta V_i^n)^2} \left(\frac{x_{i+1}^n - x_i^n}{\Delta X}\right) \left(\frac{V_{i+1}^n - V_i^n}{\Delta X}\right) = 0. \end{cases} \quad (5.16)$$

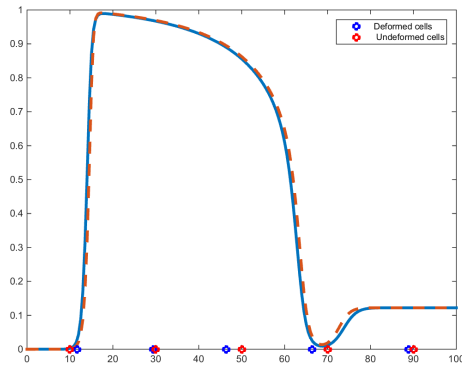
The numerical result of this model is presented in Figure 5.2. As the electrical wave propagates through the fiber, the nodes will have first a backward movement, after that a forward movement, and finally return back to their positions after the electrical signal passes away. This behavior is different than the one seen in Figure 5.1, but it is in accordance with the active-stress approach that will be observed in the next section.



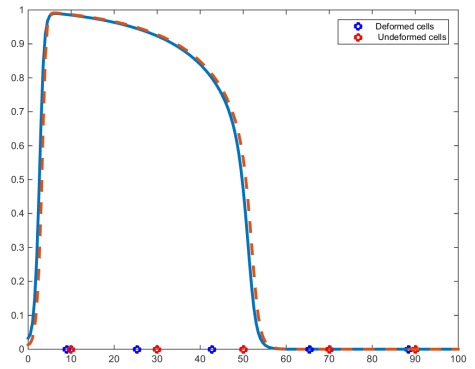
a)  $t = 0.2$



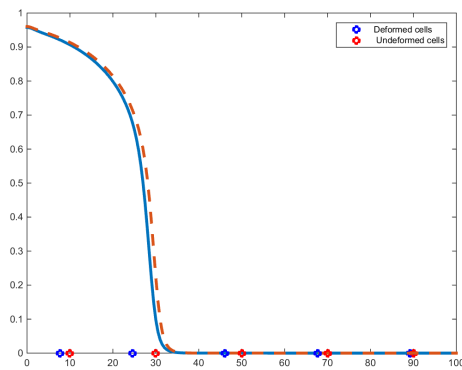
b)  $t = 23.8$



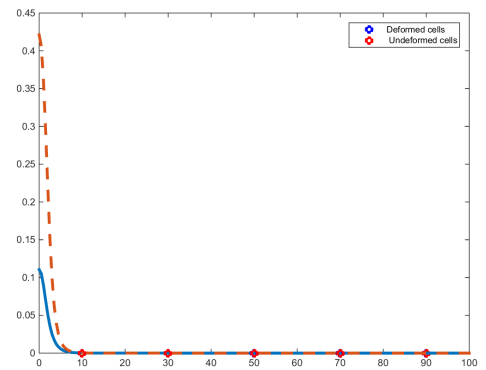
c)  $t = 39.8$



d)  $t = 47.8$



e)  $t = 63.8$



f)  $t = 83.8$

Figure 5.2: Deformation corresponding to active-strain approach: Numerical method 2

The most relevant parameter of the dynamics of the coupled electromechanical model (5.10) is  $\beta$  (L. Mesin and D. Ambrosi [24]), so we will take different values of  $\beta$  and observe what will happen as a result of numerical simulation. The numerical results are presented in Figure 5.3 at a fixed time interval where again the dashed line corresponds to the action potential before mechanics is applied and the solid line corresponds to the action potential after mechanics is applied. In this figure, we can see that for small values of  $\beta$  ( $\beta = 0.05$ ) the solid electrical wave and the dashed one coincide. But when  $\beta$  has a bigger value ( $\beta = 0.3$ ), a slight difference between the solid and dashed electrical wave is observed, and the nodes contract more by moving much forward. For high values of  $\beta$  ( $\beta = 0.4$ ), there is a remarkable difference between the dashed wave and the solid one which is interpreted as an irregular behavior [24]; moreover, we can see that the nodes contract much more than previous values of  $\beta$  by observing their forward movement.

When we change the value of  $\beta$  we change the contraction function  $\gamma$  by using equation (3.3):

$$\gamma = -\beta V,$$

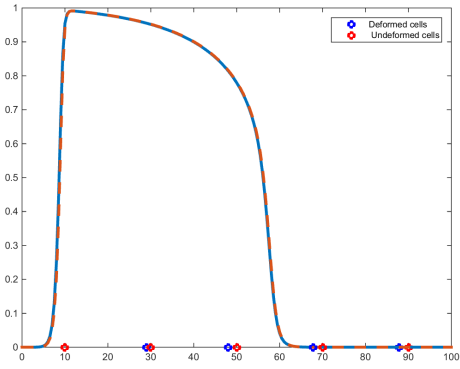
and when we change  $\gamma$ , we change the microscale part of the deformation tensor  $F_o$  by using equation (3.2):

$$F_o = 1 + \gamma.$$

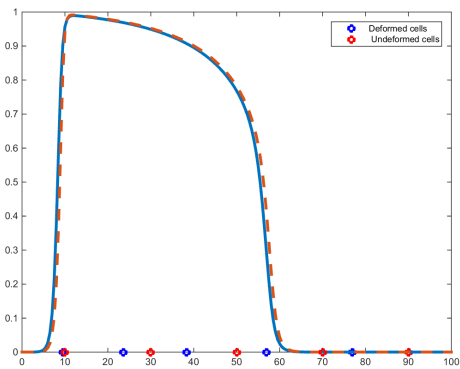
Therefore, physically changing the values of  $\beta$  allows us to adjust the magnitude of the active strain  $\mathbf{F}_o$ , which is the main factor in the mechanical equation (3.11):

$$\nabla_X \cdot (\mu J_o (\mathbf{I} + \nabla_X \mathbf{u}) \mathbf{F}_o^{-1} \mathbf{F}_o^{-T} - J p (\mathbf{I} + \nabla_X \mathbf{u})^{-T}) = 0,$$

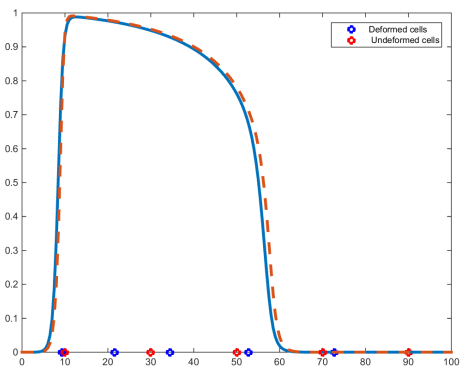
and this is considered as the main advantage of the active-strain approach model.



a)  $\beta = 0.05$



b)  $\beta = 0.3$



c)  $\beta = 0.4$

Figure 5.3: Deformation corresponding to different values of  $\beta$

## 5.2 One Dimensional Active-Stress Approach

To simplify equations given in (4.8) to a one dimensional case we use the following deformation gradient tensor  $\mathbf{F}$  in matrix form given by (A. Hazim et al. [34]):

$$\mathbf{F} = \begin{bmatrix} \frac{\partial x}{\partial X} & 0 & 0 \\ 0 & 1 & 0 \\ 0 & 0 & 1 \end{bmatrix}. \quad (5.17)$$

Recall the equation  $\mathbf{C} = \mathbf{F}^T \mathbf{F}$ , thus expressing  $tr\mathbf{C}$  as:

$$tr\mathbf{C} = \left(\frac{\partial x}{\partial X}\right)^2 + 2. \quad (5.18)$$

Substituting the value of  $\mathbf{F}$  and  $tr\mathbf{C}$  in equation (3.17), we get:

$$\begin{aligned} \mathbf{T} &= \left(2c_1 + 2c_2 \left(\left(\frac{\partial x}{\partial X}\right)^2 + 2\right)\right) \begin{bmatrix} 1 & 0 & 0 \\ 0 & 1 & 0 \\ 0 & 0 & 1 \end{bmatrix} - \\ & 2c_2 \begin{bmatrix} \left(\frac{\partial x}{\partial X}\right)^2 & 0 & 0 \\ 0 & 1 & 0 \\ 0 & 0 & 1 \end{bmatrix} + T_a \begin{bmatrix} \frac{1}{\left(\frac{\partial x}{\partial X}\right)^2} & 0 & 0 \\ 0 & 1 & 0 \\ 0 & 0 & 1 \end{bmatrix}. \end{aligned}$$

Then, the equilibrium equation (2.25) using this value of  $\mathbf{T}$  will be:

$$\frac{\partial}{\partial X} \left( \left( \left( 2c_1 + 4c_2 + \frac{T_a}{\left(\frac{\partial x}{\partial X}\right)^2} \right) \frac{\partial x}{\partial X} \right) \right) = 0. \quad (5.19)$$

But  $\frac{\partial x}{\partial X} = 1 + \frac{\partial u}{\partial X}$ .

Thus the mechanics in 1D will be given as:

$$(2c_1 + 4c_2) \frac{\partial^2 u}{\partial X^2} + \frac{1}{1 + \frac{\partial u}{\partial X}} \frac{\partial T_a}{\partial X} = 0. \quad (5.20)$$

Now the final equations of the coupled electromechanical model using the active-stress approach will be:

$$\left\{ \begin{array}{l} \frac{\partial V}{\partial t} = \mathbf{D} \frac{\partial^2 V}{\partial X^2} - kV(V - \alpha)(V - 1) - Vw - I_g, \\ \frac{\partial w}{\partial t} = \left( \epsilon + \frac{\mu_1 w}{\mu_2 + V} \right) (-w - kV(V - \alpha - 1)), \\ \frac{\partial T_a}{\partial t} = \epsilon(V) \cdot (K_{T_a} V - T_a), \\ (2c_1 + 4c_2) \frac{\partial^2 u}{\partial X^2} + \frac{1}{1 + \frac{\partial u}{\partial X}} \frac{\partial T_a}{\partial X} = 0, \end{array} \right. \quad (5.21)$$

where  $I_g$  is the stretch-activated current given by  $I_g = G_s(V - 1)(\sqrt{C} - 1)$ ,  $G_s = 0.05$  is the maximal conductance, and  $\mathbf{D}$  is the diffusion constant given by  $\mathbf{D} = \sqrt{C} \mathbf{C}^{-1} = \frac{1}{1 + \frac{\partial u}{\partial X}}$ .

We will use the semi implicit finite difference method for approximation of the solution as discussed in the previous approach. After replacement of the approximations in the system of equations (5.21), we get:

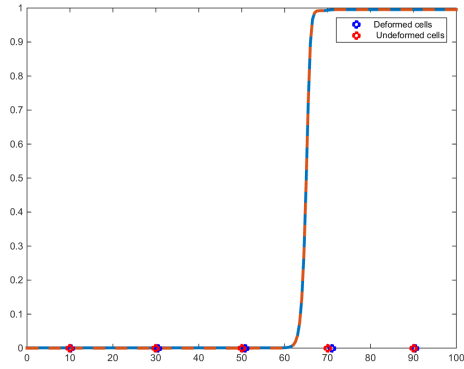
$$\left\{ \begin{array}{l} \frac{V_i^{n+1} - V_i^n}{\Delta t} = \frac{\mathbf{D}(V_{i+1}^{n+1} - 2V_i^{n+1} + V_{i-1}^{n+1})}{\Delta X^2} - kV_i^n(V_i^n - \alpha)(V_i^n - 1) - V_i^n w_i^n - I_{g_i}^n, \\ \frac{w_i^{n+1} - w_i^n}{\Delta t} = \left( \epsilon + \frac{\mu_1 w_i^n}{\mu_2 + V_i^n} \right) (-w_i^n - kV_i^n(V_i^n - \alpha - 1)), \\ \frac{T_{a_i}^{n+1} - T_{a_i}^n}{\Delta t} = \epsilon(V_i^n)(K_{T_a} V_i^n - T_{a_i}^n), \\ \frac{(2c_1 + 4c_2)(u_{i+1}^{n+1} - 2u_i^{n+1} + u_{i-1}^{n+1})}{\Delta X^2} + \left( \frac{1}{1 + \frac{u_{i+1}^n - u_i^n}{\Delta X}} \right) \left( \frac{T_{a_{i+1}}^n - T_{a_i}^n}{\Delta X} \right) = 0. \end{array} \right. \quad (5.22)$$

Same method will be used to solve for  $V$  and  $w$  as discussed in the previous approach with the same initial and boundary conditions. In this approach we have two additional equations, one for  $T_a$  and one for  $u$ . Note that  $T_a$  and  $u$  have the same initial and boundary conditions as  $w$ . The above numerical scheme has a second order accuracy in space and a first order accuracy in time; however, higher order methods can be used to avoid numerical instabilities, but we limit ourselves to first order accuracy in time since time discretization is not our goal in this thesis.

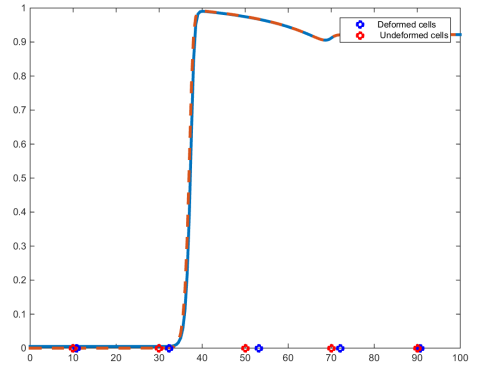
We validate our scheme by using the following analytical solution:  $V = e^{-x^2}$ ,  $w = 3e^{-x^2}$  and we get the expected order of the scheme, but for the electrical model we use the following physical parameters taken from the literature [9], given by:

parameter	$k$	$\alpha$	$\epsilon$	$\mu_1$	$\mu_2$	$K_{T_a}$	$c_1$	$c_2$
value	8	0.1	0.01	0.12	0.3	4.79	2	6

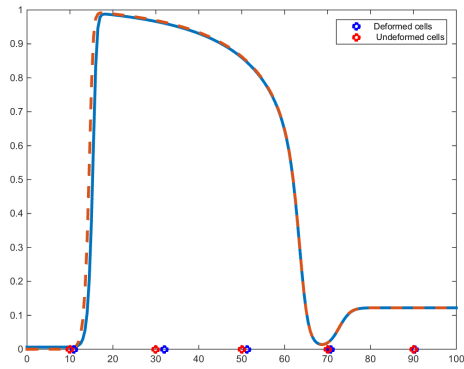
The numerical result is presented in Figure 5.4. This figure displays a sequence of time evolution of action potential  $V$ , where the dashed line corresponds to the action potential before mechanics is applied and the solid line is the action potential after mechanics is applied. To check the effect of the electromechanical coupling in the one dimensional simulation, we will fix some nodes (red dots color) on the computational domain and we observe how these nodes will deform as the electrical wave is moving. As can be seen in 5.4, as the electrical wave propagates through the fiber we will notice the backward movement of the nodes (blue dots color), then the forward movement, and at last the nodes come back to their initial position after electrical signal passes away. As a consequence, this mechanical activity has an effect on the electrical wave since the dashed line did not coincide with the solid line.



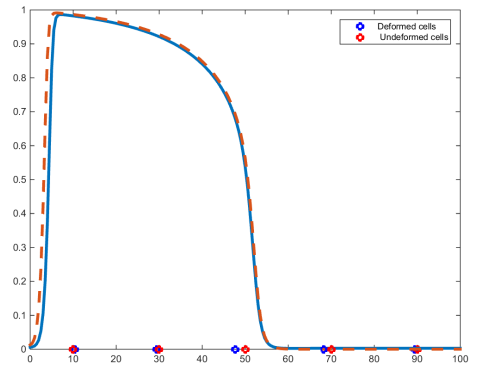
a)  $t = 3.8$



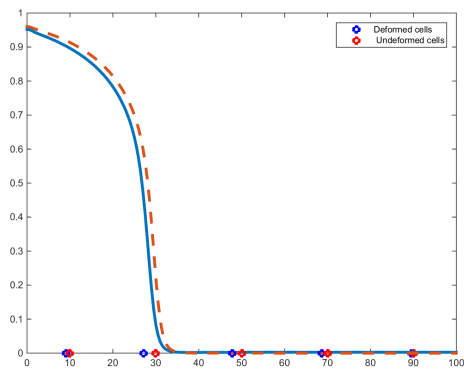
b)  $t = 23.8$



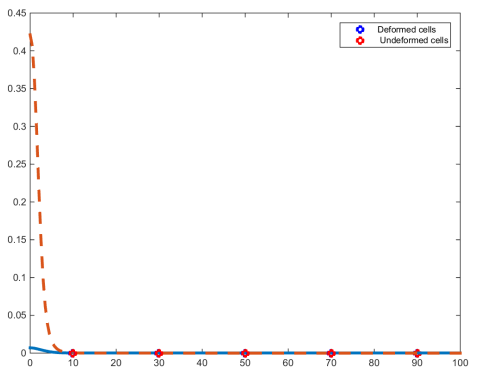
c)  $t = 39.8$



d)  $t = 47.8$



e)  $t = 63.8$



f)  $t = 83.8$

Figure 5.4: Deformation corresponding to active-stress approach

The most relevant factor for the dynamics of the coupled electromechanical model (5.21) is the active tension  $T_a$ . This active tension has two important parameters  $K_{T_a}$  and  $\epsilon(V)$ ; however, we will take different values of one parameter,  $K_{T_a}$ , and observe what will happen as a result of numerical simulation. The numerical results are presented in Figure 5.5 at a fixed time interval where again the dashed line corresponds to the action potential before mechanics is applied and the solid line corresponds to the action potential after mechanics is applied. In this figure, we can see that for small values of  $K_{T_a}$  ( $K_{T_a} = 1.79$ ) the solid electrical wave and the dashed one coincide. But when  $K_{T_a}$  has a bigger value ( $K_{T_a} = 4.79$ ), a slight difference between the solid and dashed electrical wave is observed, and the nodes contract more by moving much forward. For high values of  $K_{T_a}$  ( $K_{T_a} = 7.79$ ), there is a remarkable difference between the dashed and solid electrical wave which is interpreted as an irregular behavior; moreover, we can see that the nodes contract much more than previous values of  $K_{T_a}$  by observing their forward movement.

When we change the values of  $K_{T_a}$  we adjust the magnitude of the active tension  $T_a$  by using the following equation (4.9):

$$\frac{\partial T_a}{\partial t} = \epsilon(V)(K_{T_a}V - T_a).$$

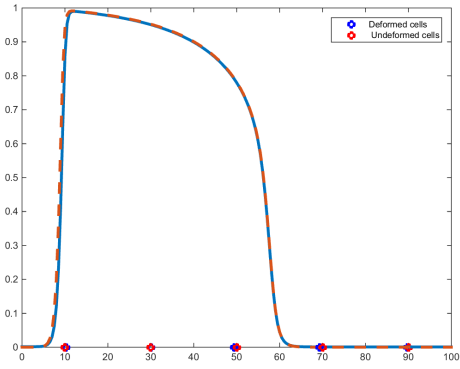
But the active tension  $T_a$  is the main factor in the mechanical equation (5.21) in the active-stress approach:

$$(2c_1 + 4c_2)\frac{\partial^2 u}{\partial X^2} + \frac{1}{1 + \frac{\partial u}{\partial X}}\frac{\partial T_a}{\partial X} = 0.$$

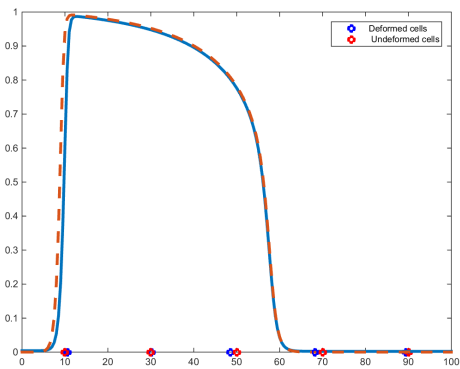
Therefore, physically changing the values of  $K_{T_a}$  allow us to adjust the magnitude of the active stress  $T_A$  by using the following formula:

$$T_A = T_a C^{-1},$$

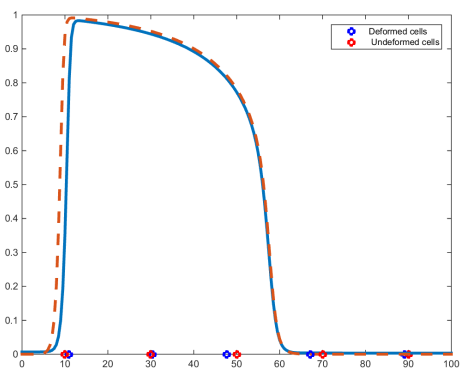
which is considered as the main contribution of the active-stress approach model.



a)  $K_{T_a} = 1.79$



b)  $K_{T_a} = 4.79$



c)  $K_{T_a} = 7.79$

Figure 5.5: Deformation corresponding to different values of  $K_{T_a}$

### 5.3 Comparison

To compare between the two approaches: active-strain and active-stress, we will differentiate between the two Figures 5.1 and 5.4. The nodes in Figure 5.1 moved only forward then came back to their initial positions; on the other hand, the nodes in Figure 5.4 moved backward, then forward and finally came back to their initial positions. Thus observing a different behavior of the nodes following the two approaches. But using the second numerical method in the active-strain approach observed in Figure 5.2, we notice exactly the same behavior as the one in the active-stress approach.

The mechanical properties of the active-strain approach can be adjusted via the contraction ratio  $\beta$  as observed in Figure 5.3, while in the active-stress approach the mechanical properties can be adjusted via the amplitude control parameter  $K_{T_a}$  as observed in Figure 5.5. Increasing the values of  $\beta$  or  $K_{T_a}$  force the electrical wave to compress and the nodes to contract more.

A deeper comparison both from mathematical and physiological point of view is still lacking as mentioned in [21]. However, some papers available in the literature addressed the advantages of the two approaches over each other. In [25], it is stated that the mathematical model of the active-strain approach is simpler than that of the active-stress; moreover, the fibers in the active-strain approach are included in the diffusion of the potential which makes this approach physiologically attractive. Above that, it is declared in [28] that the active-strain formulation does not require any added computational cost. On the other hand, the active-stress model is more flexible because of the disjunct split of passive and active parts of the stress, which is simpler experimental and interpretational wise as described in [28] since the active part of the stress tensor can be tuned to represent experimental data.

## Chapter 6: Conclusions and Future Work

The mathematical modeling of the electromechanical coupling of a cardiac tissue has been addressed by two main approaches: active-strain and active-stress. In chapter 3 we derived the mechanical equations of both approaches. These mechanical equations were coupled with the electrical equations in chapter 4, forming the coupled electromechanical models of cardiac tissues.

A numerical method for these electromechanical coupled models was proposed in chapter 5. A one-dimensional fiber simulation for both models was capable of reproducing the propagation of the electrical signal and the corresponding contraction of the nodes. Moreover, we have seen that the most relevant parameters for the dynamics of the active-strain based model and the active-stress based model are  $\beta$  and  $K_{T_a}$ , respectively.

A comparison between the two approaches was provided in section 5.3 showing the advantages of both models. We may conclude that it is beneficial if a mathematical model can be developed to utilize the advantages of both approaches and hence the mechanical properties can be adjusted via active-strain and/or active-stress parameters.

The proposed models can be extended to two and three-dimensional geometries. Also, higher order methods in space and time can be investigated for more accuracy. Finally, we stress from the modelling point of view that a deeper understanding of the electromechanical coupling is still needed and open for discussion.

## Bibliography

- [1] Finite Strain Theory, *Wikipedia*.
- [2] R. Kaufmann, R. Bayer, T. Furniss, H. Krause, and H. Tritthart. “Calcium-Movement Controlling Cardiac Contractility II. Analog Computation of Cardiac Excitation-Contraction Coupling on the Basis of Calcium Kinetics in a Multi-Compartment Model.” *Journal of Molecular and Cellular Cardiology*, vol. 6, pp. 543 – 559, 1974.
- [3] L. Waldman, Y. Fung, and J. Convell. “Transmural Myocardial Deformation in the Canine Left Ventricle: Normal in Vivo Three-Dimensional Finite Strains.” *Circulatory Research*, vol. 57, pp. 152 – 163, 1985.
- [4] R. Aliev and A. Panfilov. “A Simple Two-Variable Model of Cardiac Excitation.” *Chaos, Solutions and Fractals*, vol. 7, pp. 293 – 301, 1996.
- [5] J. Keener and J. Sneyd. *Mathematical Physiology*. Springer, New York, 1998.
- [6] P. Hunter, A. McCulloch, and H. Keurs. “Modelling the Mechanical Properties of Cardiac Muscle.” *Progress in Biophysics and Molecular Biology*, vol. 69, pp. 289 – 331, 1998.
- [7] M. Nash and P. Hunter. “Computational Mechanics of the Heart.” *Journal of Elasticity*, vol. 61, pp. 113 – 141, 2000.
- [8] J. Humphery. *Cardiovascular Solid Mechanics: Cells, Tissues, and Organs*. Springer verlag, New York, 2002.
- [9] M. Nash and A. Panfilov. “Electromechanical Model of Excitable Tissue to Study Reentrant Cardiac Arrhythmias.” *Progress in Biophysics and Molecular Biology*, vol. 85, pp. 501 – 522, 2004.
- [10] A. Panfilov, R. Keldermann, and M. Nash. “Self-Organized Pacemakers in a Coupled Reaction-Diffusion Mechanics System.” *Physical Review Letters*, vol. 95, 2005.

- [11] R. Keldermann, A. Panfilov, and M. Nash. “Pacemakers in a Reaction-Diffusion Mechanics System.” *Journal of Statistical Physics*, vol. 128, pp. 375 – 392, 2007.
- [12] P. Nardinocchi and L. Teresi. “On the Active Response of Soft Living Tissues.” *Journal of Elasticity*, vol. 88, pp. 27 – 39, 2007.
- [13] C. Cherubini, S. Filippi, P. Nardinocchi, and L. Teresi. “An Electromechanical Model of Cardiac Tissue: Constitutive Issues and Electrophysiological Effects.” *Progress in Biophysics and Molecular Biology*, vol. 97, pp. 562–573, 2008.
- [14] S. Linge, J. Sundnes, M. Hanslien, G. Lines, and A. Tveito. “Numerical Solution of the Bidomain Equations.” *Philosophical Transactions of the Royal Society A*, vol. 367, pp. 1931 – 1950, 2009.
- [15] G. Holzapfel and R. Ogden. “Constitutive Modelling of Passive Myocardium: A Structurally Based Framework for Material Characterization.” *Philosophical Transactions of the Royal Society A*, vol. 367, pp. 3445 – 3475, 2009.
- [16] P. Pathmanathan and J. Whiteley. “A Numerical Method for Cardiac Mechanoelectric Simulations.” *Annals of Biomedical Engineering*, vol. 37, pp. 860 – 873, 2009.
- [17] R. Clayton, O. Bernus, E. Cherry, H. Dierckx, F. Fenton, L. Mirabella, A. Panfilov, F. Sachse, G. Seemann, and H. Zhang. “Models of Cardiac Tissue Electrophysiology: Progress, Challenges and Open Questions.” *Progress in Biophysics and Molecular Biology*, vol. 104, pp. 22 – 48, 2010.
- [18] P. Pathmanathan, M. Bernabeu, R. Bordas, J. Cooper, A. Garny, J. Francis, J. Whiteley, and D. Gavaghan. “A Numerical Guide to the Solution of the Bidomain Equations of Cardiac Electrophysiology.” *Progress in Biophysics and Molecular Biology*, vol. 102, pp. 136 – 155, 2010.

- [19] M. Doyle, S. Tavoularis, and Y. Bourgault. “Adaptation of a Rabbit Myocardium Material Model for Use in a Canine Left Ventricle Simulation Study.” *Journal of Biomechanical Engineering*, vol. 132, pp. 1 – 12, 2010.
- [20] R. Clayton and A. Panfilov. “A Guide to Modelling Cardiac Electrical Activity in Anatomically Detailed Ventricles.” *Progress in Biophysics and Molecular Biology*, vol. 96, pp. 19 – 43, 2008.
- [21] D. Ambrosi, G. Arioli, F. Nobile, and A. Quarteroni. “Electromechanical Coupling in Cardiac Dynamics: The Active Strain Approach.” *Society for Industrial and Applied Mathematics*, vol. 71, pp. 605 – 621, 2011.
- [22] F. Nobile, A. Quarteroni, and R. Ruiz-Baier. “An Active Strain Electromechanical Model for Cardiac Tissue.” *International Journal for Numerical Methods in Biomedical Engineering*, vol. 28, pp. 52 – 71, 2011.
- [23] N. Trayanova and J. Rice. “Cardiac Electromechanical Models: From Cell to Organ.” *Journal List, Frontiers in Physiology*, vol. 2, 2011.
- [24] L. Mesin and D. Ambrosi. “Spiral Waves on a Contractile Tissue.” *The European Physical Journal Plus*, vol. 126, pp. 1 – 13, 2011.
- [25] L. Mesin. “Dynamics of Spiral Waves in a Cardiac Electromechanical Model with a Local Electromechanical Inhomogeneity.” *Chaos, Solitons and Fractals*, vol. 45, pp. 1220 – 1230, 2012.
- [26] N. Kirc. “An Adaptive, Preconditioned, Electromechanical Model for Simulation of the Cardiac Arrhythmias.” Ph.D. dissertation, *University of Leeds*, 2012.
- [27] S. Land, S. Niederer, and N. Smith. “Efficient Computational Methods for Strongly Coupled Cardiac Electromechanics.” *IEEE Transactions on Biomedical Engineering*, vol. 59, pp. 1219 – 1228, 2012.
- [28] S. Rossi, R. Baier, L. Pavarino, and A. Quarteroni. “Orthotropic Active Strain Models for the Numerical Simulation of Cardiac Biomechanics.” *In-*

- ternational Journal for Numerical Methods in Biomedical Engineering*, vol. 28, pp. 761 – 788, 2012.
- [29] F. Nobile, A. Quarteroni, R. Ruiz-Baier. “An Active Strain Electromechanical Model for Cardiac Tissue.” *International Journal for Numerical Methods in Biomedical Engineering*, vol. 28, pp. 52 – 71, 2012.
- [30] A. Gizzi, R. Baier, S. Rossi, A. Laadhari, C. Cherubini, and S. Filippi. “A Three-Dimensional Continuum Model of Active Contraction in Single Cardiomyocytes,” in *Modeling the Heart and Circulatory System*. Springer International Publishing, New York, 2013, vol. 14, ch. 6, pp. 157 – 176.
- [31] S. Goketpe, A. Menzel, and E. Kuhl. “The Generalized Hill Model: A Kinematic Approach towards Active Muscle Contraction.” *Journal of the Mechanics and Physics of Solids*, vol. 72, pp. 20 – 39, 2014.
- [32] E. Berberoglu and S. Goketpe. “Computational Modeling of Myocardial Infraction.” *Department of Civil Engineering, Procedia IUTAM*, vol. 12, pp. 52–61, 2015.
- [33] H. Dierckx, S. Arens, B. Li, L. Weise, and A. Panfilov. “A Theory for Spiral Wave Drift in Reaction-Diffusion-mechanics Systems.” *New Journal of Physics*, vol. 17, 2015.
- [34] A. Hazim, Y. Belhamadia, and S. Dubljevic. “Control of Cardiac Alternans in an Electromechanical Model of Cardiac Tissue.” *Computers in Biology and Medicine*, vol. 63, pp. 108 – 117, 2015.
- [35] R. Frotscher. “Electromechanical Modeling and Simulation of Thin Cardiac Tissue Constructs.” M.S. thesis, *Biomechanics Lab at Aachen University of Applied Sciences*, 2016.
- [36] A. Fortin and A. Garon. (2016). *Les éléments finis: de la théorie à la pratique*. [On-line]. Available: [http://giref.ulaval.ca/files/afortin/Publications/elements\\_finis.pdf](http://giref.ulaval.ca/files/afortin/Publications/elements_finis.pdf)

## **Vita**

Rana Itani was born on August 15, 1982, in Jeddah, Kingdom of Saudi Arabia. She was educated in private American schools till she finished her primary level, then she moved with her family to Beirut, Lebanon to continue her studies and took the Lebanese Baccalaureate in Sciences in 2000. After that she joined Beirut Arab University, and graduated in 2004 with a Mathematics degree, allowing her to work as a high school Math teacher for a couple of years.

Mrs. Rana got married and moved with her husband to Dubai, United Arab Emirates in 2008. She continued her career path as a Math teacher for almost five years, teaching in different international American schools. In 2015, Rana enrolled in the master program of Applied Mathematics at the American University of Sharjah where she also worked for the Department of Mathematics and Statistics as a graduate teaching assistant.